Preparation and bioactive characteristics of a porous 13–93 glass, and fabrication into the articulating surface of a proximal tibia

Qiang Fu,[1] Mohamed N. Rahaman,[1] B. Sonny Bal,[2] Wenhai Huang,[3,4] Delbert E. Day[1,3]
[1]*Department of Materials Science and Engineering, University of Missouri, Rolla, Missouri 65409*
[2]*Department of Orthopaedic Surgery, University of Missouri, Columbia, Missouri 65212*
[3]*Graduate Center for Materials Research, University of Missouri, Rolla, Missouri 65409*
[4]*School of Materials Science and Engineering, Tongji University, Shanghai 200092, China*

Received 2 February 2006; revised 12 October 2006; accepted 29 October 2006
Published online 31 January 2007 in Wiley InterScience (www.interscience.wiley.com). DOI: 10.1002/jbm.a.31156

Abstract: The silicate-based 45S5 bioactive glass, typically in particulate form, has been widely investigated for bone repair. However, its application as a scaffold for bone tissue engineering is limited due to the difficulty of forming porous three-dimensional constructs with complex shapes. In this study, the use of another silicate-based bioactive glass, referred to as 13–93, was investigated for the preparation of porous constructs. Particles of 13–93 glass (255–325 μm) were consolidated and sintered to form cylindrical constructs. Characterization of these constructs was performed using mercury porosimetry, scanning electron microscopy (SEM), and mechanical testing. Constructs with porosities of 40–45% and pore sizes in the range 100–300 μm were found to have a compressive strength of 22 ± 1 MPa. The bioactivity of the 13–93 glass was studied by immersing disks in a simulated body fluid at 37°C and characterizing the reaction products. X-ray diffraction, Fourier transform infrared (FTIR) spectroscopy, and SEM showed the formation of a crystalline hydroxyapatite layer on the glass surface after ~7 days. The ability to fabricate the complex geometrical shape of the articulating surface of a human tibia from 13–93 glass particles was demonstrated. © 2007 Wiley Periodicals, Inc. J Biomed Mater Res 82A: 222–229, 2007

Key words: bioactive glass; biomaterials, scaffold; tissue engineering

INTRODUCTION

Tissue engineering, involving the implantation of cells/tissues or stimulating host cells to grow in an implanted scaffold, has emerged as a promising approach for the regeneration of lost or damaged tissues.[1,2] The key components of this approach are a suitable supply of cells, environmental factors such as growth and differentiation supplements, and three-dimensional biomaterial scaffolds that can guide the growth of new tissue *in vitro* and *in vivo*.[3–7] Biomaterial constructs for bone tissue engineering must have a combination of desirable characteristics, such as biocompatibility, sufficient mechanical strength to support physiologic loads, and the ability to be fabricated into anatomically correct shapes.

Both ceramics and polymers have been used as scaffold materials for bone tissue engineering.[8,9] Polymers such as polylactic acid (PLA), polyglycolic acid (PGA), and their copolymers (PLGA) are degradable *in vivo*, so the scaffold can be gradually replaced by new bone matrix synthesized by tissue-forming cells.[10–13] The use of degradable polymers such as PLGA in replacing load-bearing bones is limited by their relatively low mechanical strength.[8,9] Attempts have been made to reinforce the degradable polymers to improve their load-bearing properties, but the usefulness of this approach is unclear.[14,15]

Bioactive glasses, glass-ceramics, and ceramics have been widely investigated for healing bone defects, because of their ability to enhance bone formation and bond to surrounding tissue.[16–19] Cell seeded bioactive ceramics are also of interest as potential scaffolds for bone tissue engineering. Hydroxyapatite (HA) and tricalcium phosphate (TCP) ceramics, composed of the same ions as bone, are biocompatible and produce no systemic toxicity or immunological reactions. However, stoichiometric HA resorbs slowly or undergoes little conversion to a bone-like material after implantation.[20,21] Many bone regeneration applications require gradual resorption

Correspondence to: M.N. Rahaman; e-mail: rahaman@umr.edu

of the implanted biomaterials and their concurrent replacement by the host bone.

The silicate-based 45S5 bioactive glass, referred to as Bioglass® (composition: 45 wt % SiO_2; 24.5 wt % Na_2O; 24.5 wt % CaO; 6 wt % P_2O_5), has been of primary interest for biological applications.[16,18,19] *In vivo* studies have shown that 45S5 glass can stimulate bone regeneration,[22–24] whereas *in vitro* studies have shown that the glass itself and the soluble ionic species released by dissolution have osteoinductive properties.[25–28] Porous 45S5 glass scaffolds with simple shapes have been developed[25,29] and cell culture experiments indicate that porous glass can function as a template for generating mineralization *in vitro*.[29] However, the formation of 45S5 glass into porous constructs with complex, anatomically relevant shapes is limited by the difficulty of sintering the glass particles to form a strong interconnected network.

In the present work, the use of 13–93 bioactive glass for the preparation of porous constructs for bone tissue engineering applications was investigated. The 13–93 glass (composition: 53 wt % SiO_2, 6 wt % Na_2O, 12 wt % K_2O; 5 wt % MgO, 20 wt % CaO, and 4 wt % P_2O_5) has a silicate-based composition. Previous work has shown that 13–93 glass can be melted and pulled into fibers more easily than 45S5 glass, indicating enhanced viscous flow.[30] The glass has also been shown to support cell growth.[31] The better flow characteristics and the ability to support cell growth warrant further investigation of 13–93 glass as a scaffold material for bone tissue engineering. The objectives of the present work were to investigate the processing conditions for preparing porous constructs of 13–93 glass and to characterize the structure and mechanical properties of the fabricated constructs.

MATERIALS AND METHODS

Preparation of porous 13–93 glass constructs

Glass with the 13–93 composition was prepared by melting a mixture of the appropriate quantities of analytical grade Na_2CO_3, K_2CO_3, $MgCO_3$, $CaCO_3$, SiO_2, and $NaH_2PO_4{\cdot}2H_2O$ in a platinum crucible at 1300°C and quenching between cold stainless steel plates. The glass was crushed in a hardened steel mortar and pestle and classified using stainless steel sieves to provide particles with sizes in the range of 255–325 μm.

A slip casting method was used to form the particles into three-dimensional shapes because the process has the capability for producing complex shapes by casting in a shaped mold.[32] Initially, only simple shapes such as cylinders and disks were required to determine the process variables and to characterize the fabricated material. The suspension for slip casting was prepared by dispersing 85 wt % glass particles in an aqueous solution containing 7.5 wt % poly(vinyl alcohol), PVA. Constructs were formed by casting the suspension into cylindrical cavities in a gypsum mold, followed by drying for ~24 h in air at 60°C.

The construct was heated to burn off the PVA binder, and sintered to join the glass particles together into a three-dimensional network with adequate strength. Since the glass can undergo undesirable crystallization if sintered under unsuitable conditions, experiments were carried out to determine the optimum conditions to bond the particles into a network without causing any measurable crystallization. Differential thermal analysis, DTA (Perkin Elmer DTA7, Perkin Elmer, Norwalk, CT) was used to determine the glass transition temperature (T_g) and the crystallization temperature by heating 40 mg of 13–93 glass particles (<45 μm) at a rate of 10°C/min from 50°C to 1200°C. From a series of experiments, it was found that heating the slip-cast samples at 3°C/min to 550°C (holding time = 30 min), followed by 5°C/min to 700°C (holding time = 15 min), allowed the PVA binder to be burned out completely and sintering to take place without crystallization of the glass.

The ability to use the slip casting process to form porous constructs with anatomically-correct shapes was investigated. A plastic model of the proximal articulating end of a human tibia was used to prepare the shaped cavity in a gypsum mold, into which the suspension of glass particles was cast. The procedure for fabricating the tibial construct was similar to that described above for the cylindrical samples.

Characterization of porous 13–93 glass constructs

The pore morphologies of the cylindrical constructs were observed using scanning electron microscopy, SEM (Hitachi S-4700), of the surfaces and cross-sections of the constructs. Cross-sections were prepared by infiltrating the construct with an epoxy resin under vacuum, followed by grinding with silicon carbide (SiC) paper and polishing with diamond paste. The porosity and pore size distribution of accessible (open) pores were measured using mercury intrusion porosimetry (Poremaster; Quantachrome, FL).[32] The compressive strength of cylindrical samples (8 mm in diameter × 16 mm) was measured using an Instron testing machine (Model 4204) at a crosshead speed of 0.5 mm/min. Eight samples were tested, and the average strength and standard deviation were determined.

Conversion of 13–93 glass to HA in simulated body fluid

The formation of HA on the surface of 13–93 glass disks when immersed in a simulated body fluid (SBF) at 37°C was investigated using SEM (Hitachi S-4700), X-ray diffraction, XRD (Rigaku; Model D/mas 2550 v), and Fourier transform infrared reflectance spectroscopy, FT-IRRS (Model 1760-X, Perkin Elmer, Norwalk, CT). Table I gives the composition of the SBF.[33] Glass samples with a regular geometry, such as disks, were required to facilitate the

TABLE I
Ion Concentration (mM) in SBF and in Human Blood Plasma[31]

Ion	Na^+	K^+	Mg^{2+}	Ca^{2+}	Cl^-	HCO_3^-	HPO_4^{2-}	SO_4^{2-}
SBF	142.0	5.0	1.5	2.5	147.8	4.2	1.0	0.5
Human plasma	142.0	5.0	1.5	2.5	103.0	27.0	1.0	0.5

characterization of the HA formation, particularly for short reaction times. The disks were formed by casting the molten glass into graphite molds (1 cm in diameter and 2 mm in thickness), followed by annealing for 6 h at 500°C to relieve thermal stresses. Prior to immersion in the SBF, the surfaces of the glass disks were prepared by wet grinding with 320-grit SiC paper, followed by dry grinding with 600-grit SiC paper. The samples were then cleaned in ethanol in an ultrasonic bath, and dried in air.

To study the conversion to HA, the glass disks were suspended in sealed polyethylene bottles containing 20 cm^3 of SBF, to give a sample surface area to SBF volume ratio of 0.1 cm^{-1}. After immersion in SBF for various times, the disks were dried in air at room temperature for at least 24 h. Crystalline phases formed on the surface of the glass were detected using thin-film XRD (Cu K_α radiation; $\lambda = 0.15406$ nm) at a scanning rate of 1.8°/min in the 2θ range of 10–80°. The functional groups in the reacted surface layer were analyzed using FT-IRRS in the range of 400–2000 cm^{-1}.

Following the thin film XRD and FT-IRRS characterization, cross-sections of disks soaked in SBF were prepared and observed in the SEM to characterize the thickness of the HA layer. Prior to observation in the SEM, the disks were mounted in epoxy resin, ground with SiC paper, and polished with diamond paste, using the procedure described earlier.

RESULTS AND DISCUSSION

The DTA pattern of the 13–93 glass is shown in Figure 1. Whereas the peaks and troughs are not as clearly identified as in other glasses with simpler compositions, the onset of the glass transition can be assumed to occur at 606°C. There appeared to be two crystallization events, with onset temperatures of 714°C and 851°C, respectively. Since one objective of the fabrication process was to bond the glass particles by viscous flow sintering into a porous construct without any measurable crystallization, the DTA pattern indicated that the sintering temperature should be chosen between 606 and 714°C. From preliminary experiments, it was found that sintering for 15 min at 700°C provided adequate strength for subsequent handing without any measurable crystallization of the glass. These sintering conditions were used in subsequent experiments.

Figure 2(a) shows an SEM micrograph of the surface of the porous glass construct after sintering. Joining of the particles at the contact points resulted in the formation of necks [Fig. 2(b)] that produced an interconnected network with enhanced strength. A cross-section [Figure 2(c)] shows the network of bonded glass particles and porosity. Mercury porosimetry data (Fig. 3) showed that the porosity of the sintered constructs, determined from the volume of mercury intruded divided by the total volume of the sample, was 40 ± 2%. By taking the volume intruded for pore radius values between 50 and 150 μm and dividing by the total volume intruded, it was found that ~75% of the interconnected pores had channel diameters between 100 and 300 μm. Similarly, it was found that ~90% of the pores had channel diameters larger than 100 μm. Generally, it has been found that pores larger than ~100 μm are capable of supporting cell ingrowth.[34,35] Thus, the pores in the present constructs appear to have dimensions that are suitable for biomedical scaffolds.

The compressive strength of porous cylindrical samples was 22 ± 1 MPa. This value is significantly higher than the value for cancellous bone (2–12 MPa), but it is also significantly lower than that for cortical bone (100–200 MPa). While the design criteria for scaffolds for bone tissue engineering are unclear, it should be noted that the strength of the present constructs can be enhanced by a greater degree of sintering, at the expense of some reduction in the porosity and average pore size. It is possible that sintering at a higher temperature or for a longer time could lead to crystallization of the glass. However, the preliminary studies in the present work indicated that sintering for 15 min at 710°C, which is 10°C higher than the temperature used in the experiments reported here, produced more rapid sintering without detectable crystallization. Based on data for 45S5 bioactive glass,[36] a limited extent of crystallization would not affect the ability to bond to bone,

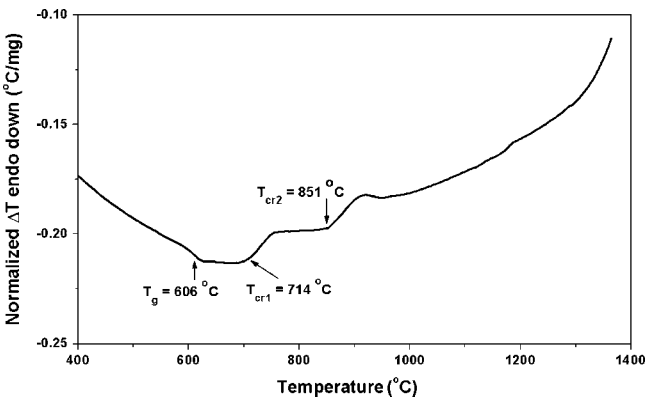

Figure 1. Differential thermal analysis of 13–93 glass, showing the glass transition and crystallization regions.

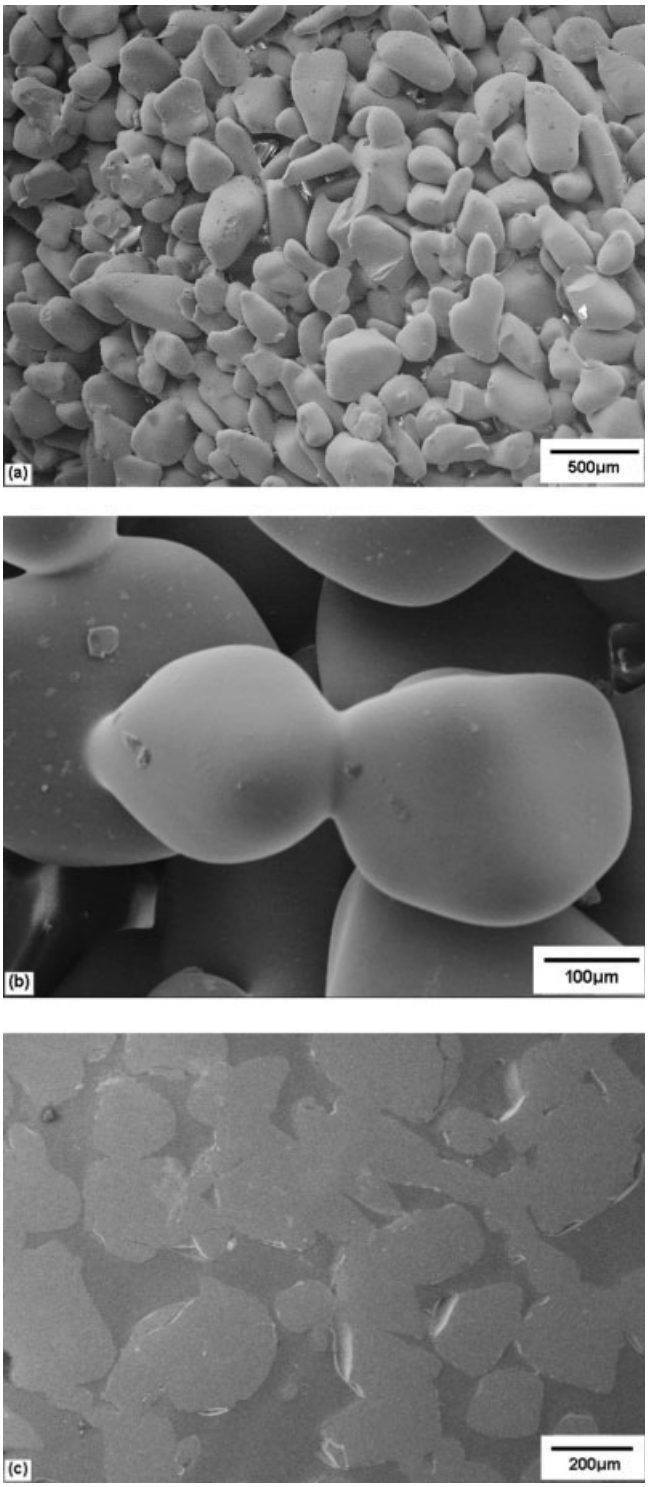

Figure 2. SEM of (a) the surface of a porous glass construct prepared by sintering, (b) the neck region between two particles, showing bonding between the particles, and (c) a cross-section of the construct showing the bonded particles and pores.

although the rate of formation of HA would be reduced.

Thin-film XRD patterns for the as-prepared glass and for the glass after soaking in SBF for 1, 7, and

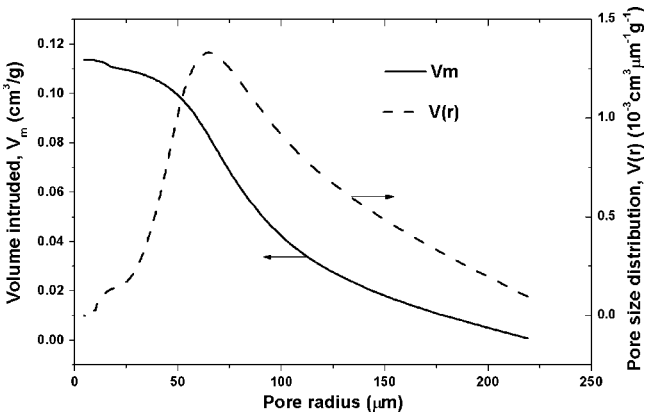

Figure 3. Mercury porosimetry of the fabricated constructs, showing the pore volume and the pore size distribution as functions of the pore radius.

14 days are shown in Figure 4. The as-prepared glass showed the commonly observed band centered at $\sim 30^\circ$ 2θ, which is typical of an amorphous glass. After 1 day in the SBF, the pattern became almost flat. A possible reason for the disappearance of the broad band, previously observed for the as-prepared glass, is the formation of an amorphous product on the surface of the glass. The thin-film technique analyzed the amorphous reaction layer, and not the underlying glass. After 7 days, peaks corresponding to those for a standard HA were observed. These peaks increased in intensity after 14 days of immersion, but the peak intensities were still well below those for a standard crystalline HA, indicating that the as-formed HA was incompletely crystallized or only weakly crystalline.

The FT-IRRS spectra (Fig. 5) demonstrated that the major resonances associated with crystalline HA, at wavenumbers of 560 and 605 cm^{-1},[37,38] were observed for the glass soaked in SBF for 7 days but not for the as-prepared glass, providing further indication for the formation of an HA layer on the sur-

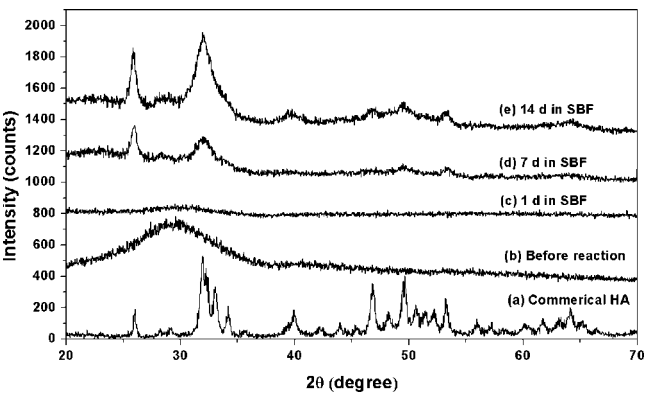

Figure 4. Thin-film XRD of the 13–93 glass, and the glass after immersion in a simulated body fluid at 37°C for various times.

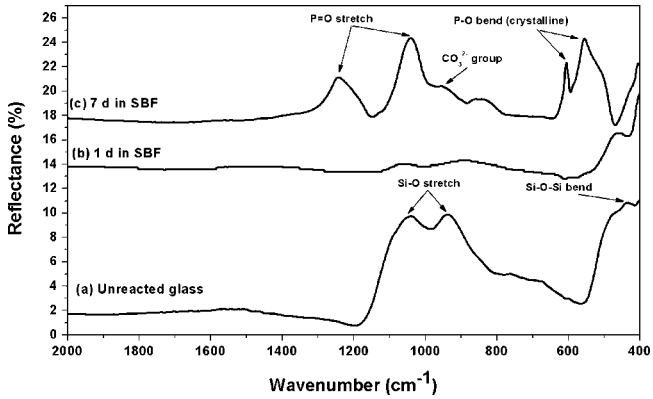

Figure 5. FTIR of the 13–93 glass and the glass after immersion in a simulated body fluid at 37°C for various times.

face of the glass soaked in SBF. The spectrum for the as-prepared glass showed resonances at 1050 and 940 cm^{-1} attributed to the stretching vibration modes of Si bonded to nonbridging O in the glass network, as well as a resonance at 440 cm^{-1} corresponding to the bending vibration of the Si-O-Si bond. The spectrum for the glass soaked in SBF for 7 days also showed resonances at 1030 and 1243 cm^{-1} corresponding to the phosphate group. There was a resonance at 866 cm^{-1} as well, corresponding to the stretching vibration of CO_3^{2-} function group, which indicated that the as-formed HA had carbonate groups substituted into the structure.[39] The FT-IRRS spectra therefore indicated that the surface of the glass soaked in SBF was coated with a carbonate-substituted HA layer.

Figure 6(a,b) shows SEM micrographs of the cross-sections of the 13–93 glass prior to immersion in SBF and after immersion for 14 days. Micrographs were also obtained for immersion times of 1 day and 7 days but they are omitted for the sake of brevity. The as-formed HA layer in Figure 6(b) suffered from a greater degree of degradation during the sample preparation step (grinding and polishing of the cross-section), which accounted for the rough nature of the layer seen in the micrograph. The thickness of the HA formed after each immersion in SBF was determined from at least five SEM micrographs of the cross-section. Figure 7 shows data for the HA thickness versus the immersion time in SBF. Within the limits of experimental error, the growth of the HA layer was linear, increasing at a rate of $\sim$0.4 μm per day. Since the HA product was porous, it might be expected that the diffusion of ions through the liquid in the pores of the HA would be fast, so the reaction at the planar interface between the HA and the glass would be rate-controlling. For an interface reaction-controlled mechanism, a linear increase in the reaction layer thickness would be expected, as indeed observed in Figure 7.

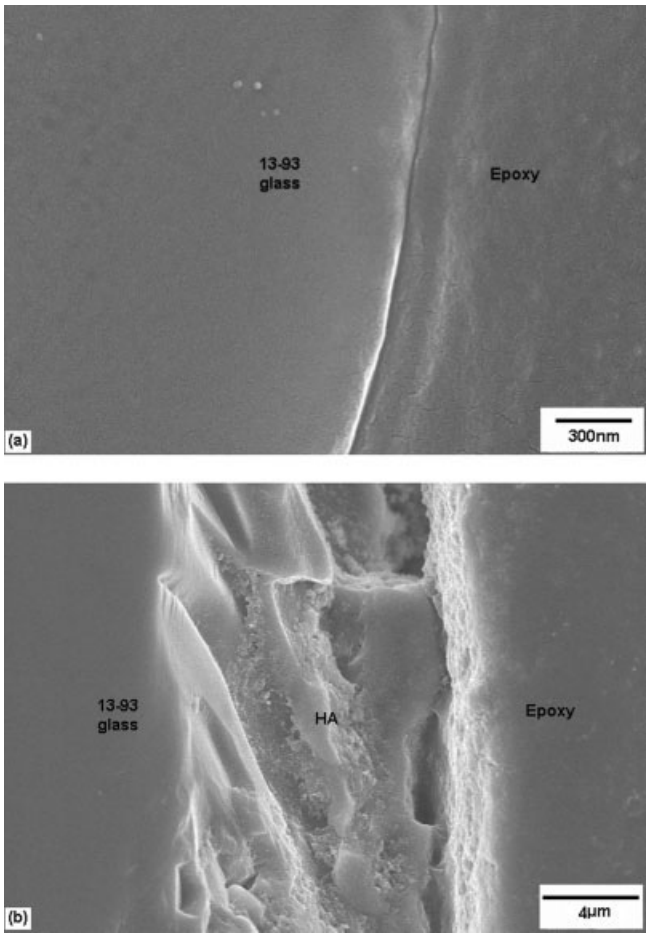

Figure 6. SEM micrographs of the cross-sections of the 13–93 glass (a) prior to immersion, and (b) after immersion for 14 days in a simulated body fluid at 37°C, showing the hydroxyapatite layer.

The mechanism of conversion of silicate-based bioactive glasses, such as 45S5 glass, in a dilute phosphate solution, such as an SBF, has been discussed

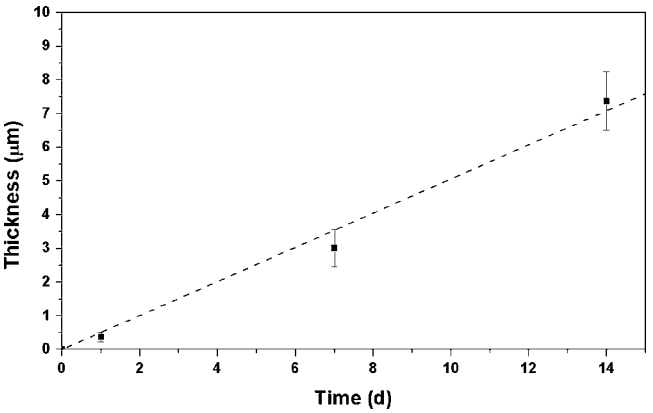

Figure 7. Thickness of the hydroxyapatite layer formed on the 13–93 glass as a function of the immersion time in a simulated body fluid at 37°C. (Linear regression: $r = 0.9954$; $p < 0.0001$).

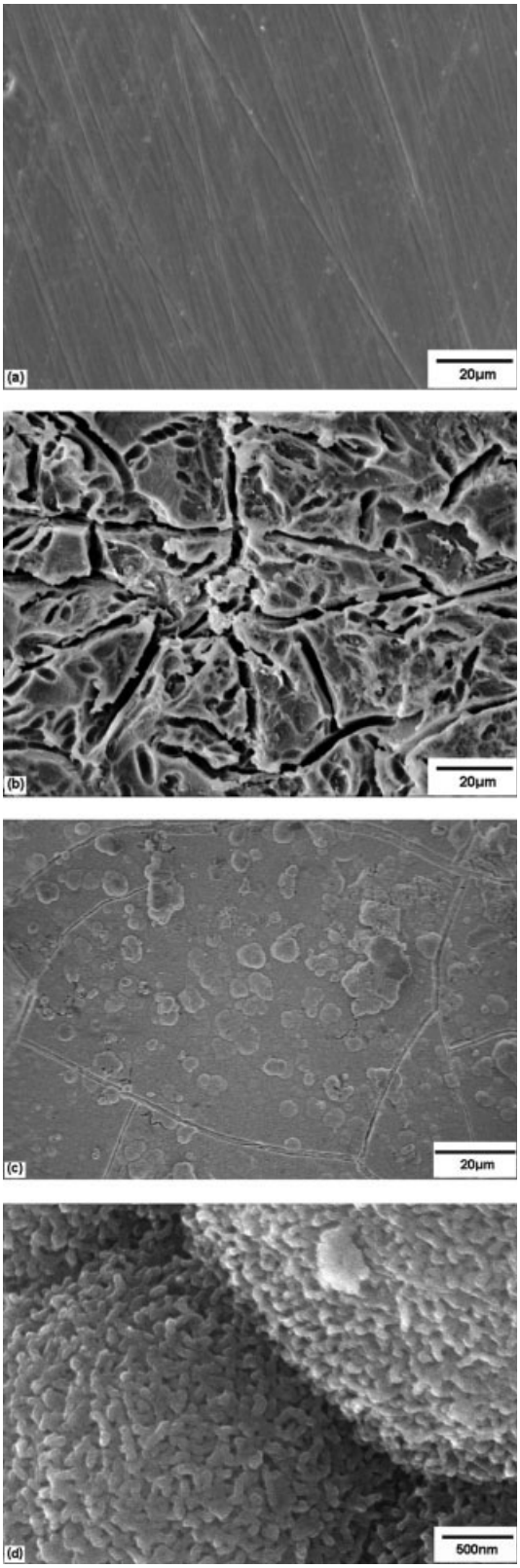

Figure 8. SEM of (a) the surface of 13–93 glass, and the surface after immersing the glass in a simulated body fluid for 1 day (b), and 7 days (c). A high magnification micrograph of the surface (7 days immersion) is shown in (d).

by Hench.[17–19] It is expected that a similar mechanism would operate for the silicate-based 13–93 glass used in the present work because it is based on the 45S5 composition. The present work provided information on the structure and characteristics of the HA formed on the 13–93 glass surface, as well as the rate at which the HA layer formed. Recent data for the conversion of particles of 45S5 glass and 13–93 glass at 37°C in 0.02 M K_2HPO_4 solution with a pH of 7.0 indicated that the formation of HA was slower for the 13–93 glass than for the 45S5 glass.[40,41]

Figure 8 shows SEM micrographs of the surface of the glass prior to, and after immersion in the SBF. Except for scratches and grooves resulting from the grinding process, the surface of the glass was flat and featureless [Fig. 8(a)]. After one day [Fig. 8(b)], the surface of the glass was covered with a reaction layer, shown earlier by thin-film XRD to be amorphous. The reaction layer (but not the underlying glass) contained cracks, typical of capillary-induced drying cracks. After 7 days [Fig. 8(c)], the glass surface was covered with a reaction layer on which another layer of precipitates were forming. The reaction layer, shown earlier to consist of a carbonate-substituted HA, also contained typical drying cracks. High-resolution SEM [Figure 8(d)] showed that the precipitates consisted of a porous network of nanoscale crystals, not unlike the rod-like HA crystals in human bone.

The ability to fabricate 13–93 glass particles into a complex shape was demonstrated by using the articulating surface of a proximal human tibia as a model. Figure 9 shows a [1/4] scale model of the tibial surface, measuring $\sim 1.5 \times 1$ inch, with a thick-

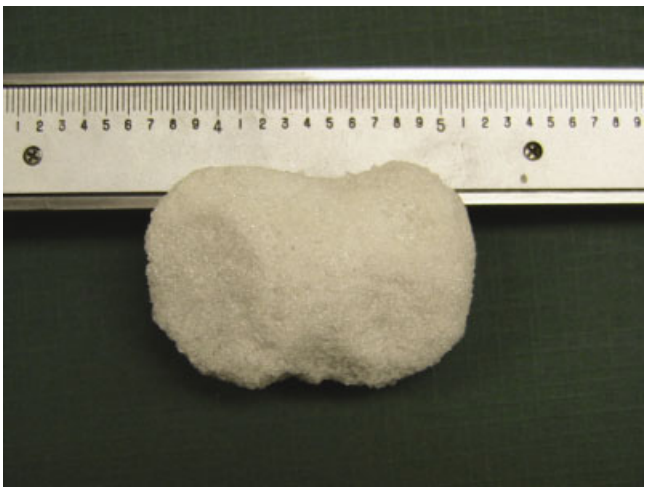

Figure 9. Optical micrograph of a porous construct with the shape of the articulating surface of a human proximal tibia prepared by slip casting and sintering 13–93 glass particles. [Color figure can be viewed in the online issue, which is available at www.interscience.wiley.com.]

ness of 0.5 inch. Since the tibial construct was prepared using the same conditions described previously, the structure, mechanical properties, and chemical properties should be almost identical to those described earlier for the cylindrical samples.

The present work demonstrated that 13–93 glass particles can be formed into constructs with the porous structure and complex shape suitable for applications in bone tissue engineering. Future work will examine the *in vitro* interaction with cells and the *in vivo* behavior of the glass constructs.

SUMMARY AND CONCLUSIONS

Porous cylindrical constructs of a silicate-based 13–93 glass were prepared using a process involving slip-casting and sintering of particles (255–325 μm). The cylinders had a porosity of 40–45%, with the majority of the pores having sizes in the range of 100–300 μm. The compressive strength of the porous cylinders was 22 ± 1 MPa. Upon immersion in a SBF at 37°C, a carbonate-substituted HA was detected on the glass surface in less than 7 days, indicating the bioactivity of the glass and the potential for bonding to bone. The rate of formation of the HA layer on the glass was ~0.5 μm per day. The ability to form a porous construct with the shape of a human tibia was demonstrated. The bioactivity of 13–93 glass, coupled with the ability to make porous constructs with anatomically correct dimensions, indicates the suitability of this material for applications in bone tissue engineering.

References

1. Nerem RM. Cellular engineering. Ann Biomed Eng 1991; 19:529–545.
2. Langer R, Vacanti JP. Tissue engineering. Science 1993;260: 920–926.
3. Vacanti JP, Langer R. Tissue engineering: The design and fabrication of living replacement devices for surgical reconstruction and transplantation. Lancet 1999;354 (Suppl 1):32–34.
4. Langer R, Vacanti JP. Tissue engineering: The challenges ahead. Sci Am 1999;280:86–89.
5. Mooney DJ, Mikos AG. Growing new organs. Sci Am 1999; 280:60–65.
6. Stock UA, Vacanti JP. Tissue engineering: Current state and prospects. Annu Rev Med 2001;52:443–451.
7. Vats A, Tolley NS, Polak JM, Gough JE. Scaffolds and biomaterials for tissue engineering: A review of clinical applications. Clin Otolaryngol 2003;28:165–172.
8. Goldstein SA, Patil PV, Moalli MR. Perspectives on tissue engineering of bone. Clin Orthop Relat Res 1999; (Suppl 357): S419–S423.
9. Kneser U, Schaefer DJ, Munder B, Klemt C, Andree C, Stark GB. Tissue engineering of bone. Min Invas Ther Allied Technol 2002;11:107–116.
10. Griffith LG. Polymeric biomaterials. Acta Mater 2000;48:263–277.
11. Agrawal CM, Ray RB. Biodegradable polymer scaffolds for musculoskeletal tissue engineering. J Biomed Mater Res 2001; 55:141–150.
12. Holy CE, Shoichet MS, Davi JE. Engineering three-dimensional bone tissue *in vitro* using biodegradable scaffolds: Investigating initial cell-seeding density and culture period. J Biomed Mater Res 2000;51:376–382.
13. Borden M, El-Almin SF, Attawia M, Laurencin CT. Structural and human cellular assessment of a novel microsphere-based tissue engineered scaffold for bone repair. Biomaterials 2003; 24:597–609.
14. Zhang R, Ma PX. Poly(α-hydroxyl acids)/hydroxyapatite porous composites for bone-tissue engineering. I. Preparation and morphology. J Biomed Mater Res 1999;44:446–455.
15. Thomson RC, Yaszemski MJ, Powers JM, Mikos AG. Hydroxyapatite fiber-reinforced poly(α-hydroxy ester) foams for bone regeneration. Biomaterials 1998;19:1935–1943.
16. Hench LL, Wilson J. Surface active biomaterials. Science 1984; 226:630–636.
17. Yamamuro T, Hench LL, Wilson J, editors. Handbook of Bioactive Ceramics. Vol. 1 and 2. Boca Raton, FL: CRC Press; 1990.
18. Hench LL. Bioceramics: From concept to clinic. J Am Ceram Soc 1991;74:1487–1510.
19. Hench LL. Bioceramics. J Am Ceram Soc 1998;81:1705–1728.
20. Klein C, Patka P, den Hollander W. Macroporous calcium phosphate bioceramics in dog femora: A histological study of interface and biodegradation. Biomaterials 1989;10:59–62.
21. Martin RB, Chapman MW, Sharkey NA, Zissimos SL, Bay B, Shors EC. Bone ingrowth and mechanical properties of coralline hydroxyapatite 1 yr after implantation. Biomaterials 1993; 14:341–348.
22. Wheeler DL, Stokes KE, Park HM, Hollinger JO. Evaluation of particulate Bioglass® in a rabbit radius ostectomy model. J Biomed Mater Res 1997;35:249–254.
23. Wheeler DL, Stokes KE, Hoellrich RG, Chamberland DL, McLoughlin SW. Effect of bioactive glass particle size on osseous regeneration of cancellous defects. J Biomed Mater Res 1998;41:527–533.
24. Oonishi H, Hench LL, Wilson J, Sugihara F, Tsuji E, Kushitani S, Iwaki H. Comparative bone growth behavior in granules of bioceramic materials of various sizes. J Biomed Mater Res 1999;44:31–43.
25. Effah Kaufmann EAB, Ducheyne P, Shapiro IM. Evaluation of osteoblast response to porous bioactive glass (45S5) by RT-PCR analysis. Tissue Eng 2000;6:19–28.
26. Silver IA, Deas J, Erecińska M. Interactions of bioactive glasses with osteoblasts in vitro: Effects of 45S5 Bioglass®, and 58S and 77S bioactive glasses on metabolism, intracellular ion concentrations and cell viability. Biomaterials 2001;22: 175–185.
27. Xynos ID, Hukkanen MVJ, Batten JJ, Buttery LD, Hench LL, Polak JM. Bioglass® 45S5 stimulates osteoblast turnover and enhances bone formation in vitro: Implications and applications for bone tissue engineering. Calcif Tissue Int 2000;67: 321–329.
28. Xynos ID, Edgar AJ, Buttery LDK, Hench LL, Polak JM. Gene-expression profiling of human osteoblasts following treatment with the ionic products of Bioglass® 45S5 dissolution. J Biomed Mater Res 2001;55:151–157.
29. El-Ghannam A, Ducheyne P, Shapiro IM. A bioactive glass template for *in vivo* synthesis of bone. J Biomed Mater Res 1995;29:359–370.
30. Paatola T, Pirhonen E, Törmälä P. Coating of bioactive glass (13–93) fibers with bioabsorbable polymer. Key Eng Mater 2001;192–195:717–720.
31. Brink M, Turunen T, Happonen RP, Yli-Urpo A. Compositional dependence of bioactivity of glasses in the system

Na_2O-K_2O-MgO-CaO-B_2O_3-P_2O5-SiO_2. J Biomed Mater Res 1997;37:114–121.
32. Rahaman MN. Ceramic Processing and Sintering, 2nd ed. New York:Marcel Dekker; 2003.
33. Kokubo T, Kushitani H, Sakka S, Kitsugi T, Yamamuro T. Solutions able to reproduce in vivo surface-structure changes in bioactive glass ceramic A-W. J Biomed Mater Res 1990; 24:721–734.
34. Freyman TM, Yannas IV, Gibson LJ. Cellular materials as porous scaffolds for tissue engineering. Prog Mater Sci 2001;46: 273–282.
35. Murphy W, Dennis RG, Kileny JL, Mooney DJ. Salt fusion: An approach to improve pore interconnectivity within tissue engineering scaffolds. Tissue Eng 2002;8:43–52.
36. Hench LL, Paschall HA. Direct chemical bonding between bioactive glass-ceramic materials and bone. J Biomed Mater Res 1973;4:25–42.
37. Clark AE, Hench LL. Early stages of calcium-phosphate layer formation in bioglass. J Non-Cryst Solids 1989;113:195–202.
38. Filgueiras MR, LaTorre G, Hench LL. Solution effects on the surface reaction of a bioactive glass. J Biomed Mater Res 1993;27:445–453.
39. Morgan H, Wilson RM, Elliott JC, Dowker SEP, Anderson P. Preparation and characterization of monoclinic hydroxyapatite and its precipitated carbonate apatite intermediate—A combined IR and XRD Rietveld analysis. Biomaterials 2000; 21:617–627.
40. Huang W, Day DE, Kittiratanapiboon K, Rahaman MN. Kinetics and mechanism of the conversion of silicate (45S5), borate, and borosilicate glasses to hydroxyapatite in dilute phosphate solutions. J Mater Sci Mater Med 2006;17:583–596.
41. Yao A, Wang D, Fu Q, Huang W, Rahaman MN, Day DE. In vitro bioactive characteristics of borate-based glasses with controllable degradation behavior. J Am Ceram Soc 2007. In Press.